Front. Mech. Eng. 2022, 17(3): 38
https://doi.org/10.1007/s11465-022-0694-2

RESEARCH ARTICLE

Energy saving design of the machining unit of hobbing machine tool with integrated optimization

Yan LV[a], Congbo LI (✉)[a], Jixiang HE[b], Wei LI[a], Xinyu LI[c], Juan LI[a]

[a] *State Key Laboratory of Mechanical Transmission, College of Mechanical and Vehicle Engineering, Chongqing University, Chongqing 400044, China*
[b] *Department of Process Technology, Sichuan Aerospace Fenghuo Servo Control Technology Corporation, Chengdu 611130, China*
[c] *State Key Laboratory of Digital Manufacturing Equipment and Technology, Huazhong University of Science and Technology, Wuhan 430074, China*

✉ *Corresponding author. E-mail: congboli@cqu.edu.cn (Congbo LI)*

ABSTRACT The machining unit of hobbing machine tool accounts for a large portion of the energy consumption during the operating phase. The optimization design is a practical means of energy saving and can reduce energy consumption essentially. However, this issue has rarely been discussed in depth in previous research. A comprehensive function of energy consumption of the machining unit is built to address this problem. Surrogate models are established by using effective fitting methods. An integrated optimization model for reducing tool displacement and energy consumption is developed on the basis of the energy consumption function and surrogate models, and the parameters of the motor and structure are considered simultaneously. Results show that the energy consumption and tool displacement of the machining unit are reduced, indicating that energy saving is achieved and the machining accuracy is guaranteed. The influence of optimization variables on the objectives is analyzed to inform the design.

KEYWORDS energy saving design, energy consumption, machining unit, integrated optimization, machine tool

1 Introduction

Manufacturing has created a considerable wealth and brought numerous jobs to the world [1]. However, it has caused serious environmental effects, such as energy shortage and climate warming. Worldwide energy consumption and carbon dioxide emissions are projected to increase by 56% and 46% between 2010 and 2040 [2], and manufacturing currently accounts for more than 30% of the world's total energy use and releases 36% of total carbon dioxide emissions [3]. The manufacturing industry is facing a difficult undertaking of energy saving and emission reduction to reach the target of global carbon neutrality. Therefore, energy saving and low-carbon development have become the inevitable choice for future manufacturing.

Machine tools are the core equipment in manufacturing. On the one hand, the energy consumption of machine tools accounts for 75% of the energy consumption in manufacturing [4], but the energy efficiency of machine tools is only 10%–15% [5]. On the other hand, environmental studies of machine tools show that more than 99% of the environmental effect is caused by electricity consumption [6]. In summary, machine tools have great potential for energy saving, and improving the energy efficiency of machine tools can remarkably reduce the energy consumption and environmental emissions of the manufacturing industry.

A review of current literature shows that many studies focused on the energy consumption modeling of machine tools. Some researchers attempted to build the energy consumption function of machine tools through theoretical deduction. In Ref. [7], an energy consumption function of the machining center in the milling process was deduced by analyzing the energy flow characteristics of the machining center processing system. Reference [8] comprehensively analyzed the mechanism of process parameters and relative cutting specific energy, and built the models of cutting force and specific cutting energy. Xiao et al. [9] developed a multicomponent energy model based on the energy characteristic analysis of dry gear hobbing machines. Energy consumption modeling based

Received October 14, 2021; accepted April 11, 2022

on theoretical deduction has minimal dependence on data, good interpretability, and can obtain specific energy consumption functions. However, the deduction process is cumbersome and has many parameters and complex calculations.

Some studies established energy consumption models by using experimental data and surrogate model methods. Li et al. [10] used Taguchi method to design the experiment and applied response surface methodology (RSM) to develop surrogate models for the specific energy consumption based on the experimental data. Vu et al. [11] applied kriging and RSM surrogate models to generate approximate regression models and showed the relationship between the parameters of hard milling and outputs (cutting energy, surface roughness, etc.) obtained by physical experiments. In Ref. [12], a radial basis function (RBF) neural network was used to render the relationships between milling processing parameters and measured performance (energy efficiency, surface roughness, etc.). Arriaza et al. [13] obtained a quantitative form of the relationship between the factors and responses by utilizing RSM and the desirability function method. The independent factors included the spindle speed, feed rate, depth, and cutting width, and the responses are the consumed energy and machining time. Energy consumption modeling based on data and surrogate models has the advantages of simple process, high modeling speed, and good accuracy, but it greatly depends on data and has poor process visibility.

The above two types of energy consumption modeling methods have their own advantages and disadvantages, and their applicable conditions are different. They are effective method for energy consumption modeling and analysis.

Numerous researchers have investigated the energy saving optimization of machine tools based on energy consumption analysis and modeling, which can be divided into two parts: processing strategy optimization and machine tool design optimization [14]. Many of the investigations have focused on the processing parameter optimization problems and adopted the multiobjective optimization algorithms to solve the problems.

A multiobjective cutting parameter optimization model that took the machining surface roughness, material removal rate, and machining energy consumption as the optimization objectives was established in Ref. [15], and an improved teaching-learning-based optimization algorithm was proposed to solve the model under various limited milling conditions. Zhang et al. [16] built a parameter optimization model of micromilling process, and used hybrid cuckoo search and grey wolf algorithm to determine the optimal cutting parameters for minimizing the total energy consumption. He et al. [17] optimized the cutting parameters with the objectives of machining efficiency, cutting force, and energy consumption, and used various algorithms, including sharing function approach, vector evaluated genetic algorithm, nondominated sorting genetic algorithm-II, and multiobjective evolutionary algorithm based on decomposition, to study the Pareto front. Kumar et al. [18] studied the multiobjective optimization of prime energy consumption responses along with material removal rate and surface roughness on rough turning. The multiperformance composite index was determined by using the technique for order preference by similarity to ideal solution method, and the weights of responses were obtained by using the equal, analytic hierarchy process, and entropy weight methods. However, the energy saving effect achieved through the optimization of processing parameters is limited, and processing parameter optimization can only achieve energy saving of existing machine tools. The energy saving design of machine tools must be investigated to improve the energy efficiency of machine tools in the design stage.

Energy saving design of machine tools has become an important direction and research frontier for the sustainable development of manufacturing in the world. An international standard “Design methodology for energy-efficient machine tools” (ISO 14955-1) has been released, providing the framework and principles of energy saving design. The European Commission has adopted a series of policies, including the ECODESIGN Directive and Energy Efficiency Directive to formulate ecodesign guidelines [19]. Energy saving design of machine tools is an important means for the manufacturing sectors to implement the concept of energy saving and low-carbon development, and is an important development trend for the machine tool industry in the future.

Several studies have been conducted to emphasize the possibility of energy saving in the design stage of machine tools. Some researchers attempted to improve the energy efficiency of machine tools by optimizing the component structures and motor parameters. Triebe et al. [20] reduced the mass and deflection of the machine table by optimizing its structure, which can help to achieve energy saving of the machine tool. Ji et al. [21] presented an optimization design method of the feed system for energy saving. The energy saving of the machine tool is realized by optimizing the structural parameters of the moving component. Some studies tried to reduce the energy consumption of machine tools by optimizing the parameters of motors. Lv et al. [22] proposed that the energy consumption will decrease if the motor can be prevented from unnecessary stopping and restarting, thereby shortening the acceleration time. The results indicate that the energy consumption can be reduced by 10.6% to more than 50%. Wójcicki and Bianchi [23] found that energy savings can be achieved in terms of peak power and energy loss by using the best acceleration rate and power limit value.

Structure and motor parameter optimizations are currently studied separately to reduce energy

consumption. Minimal studies have investigated the energy saving of machine tools by combining the optimization of structure and motor parameters, and few studies have focused on the optimization design of machine tools for energy saving.

The main contributions of this paper are as follows: 1) Compared with previous studies that achieved the energy saving of machine tools during the operating phase, this work attempts to improve the energy efficiency of hobbing machine tools in the design stage and proposes an energy saving design method. 2) A combination of theoretical formulas and surrogate models is used to establish a comprehensive energy consumption function for calculating the complex energy consumption of the main drive and feed system of the machining unit. An integrated optimization model of the machining unit considering the motor and structure parameters is proposed, and the energy consumption is reduced while ensuring machining accuracy. 3) The influence of the optimization variables on the objectives is analyzed and discussed in detail, which can improve the basis for energy saving design of machine tools.

The rest of this article is organized as follows. Section 2 established the energy consumption function of the machining unit of hobbing machine tool. Section 3 built the surrogate models of the tool post support plate mass and tool displacement, and presents the integrated optimization model. Section 4 discussed the optimization results and comparative analysis. Section 5 presented the conclusions and future research issues. The flowchart of the whole article is shown in Fig. 1.

2 Energy consumption function of the machining unit

The main drive and feed system are the main parts of machine tools, which remarkably affect the machining performance and energy efficiency of machine tools [24]. The components closely related to the machining of hobbing machine tools, including spindles and motors, make up the machining unit.

As shown in Fig. 2, the machining unit of the computer numerical control (CNC) hobbing machine tool mainly includes the main motor, servo motor, hob, tool post shell, tool post support plate, slide plate, and main gearbox. The machining unit is driven by the main motor and the servo motor. The output torque of the main motor

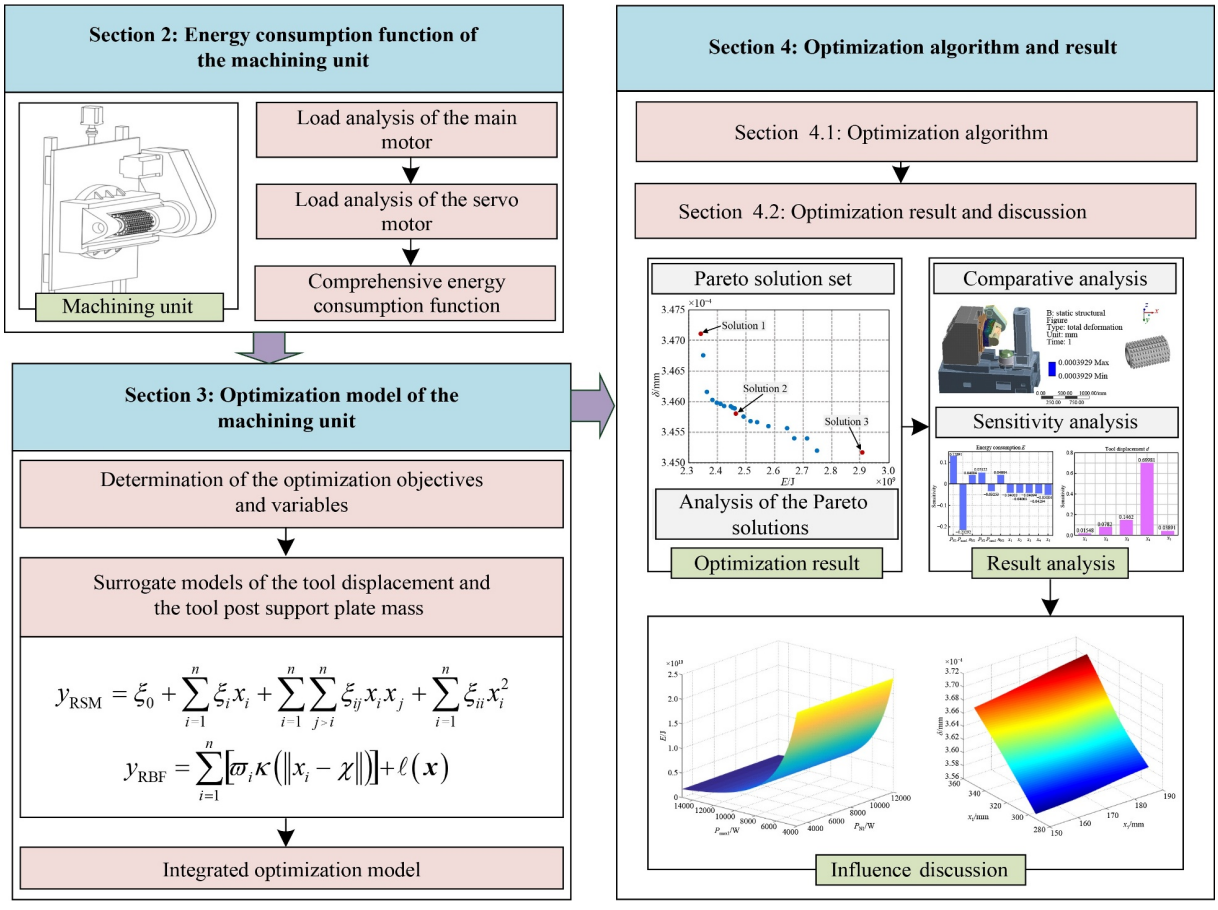

Fig. 1 Flow chart of the energy saving design of the machining unit.

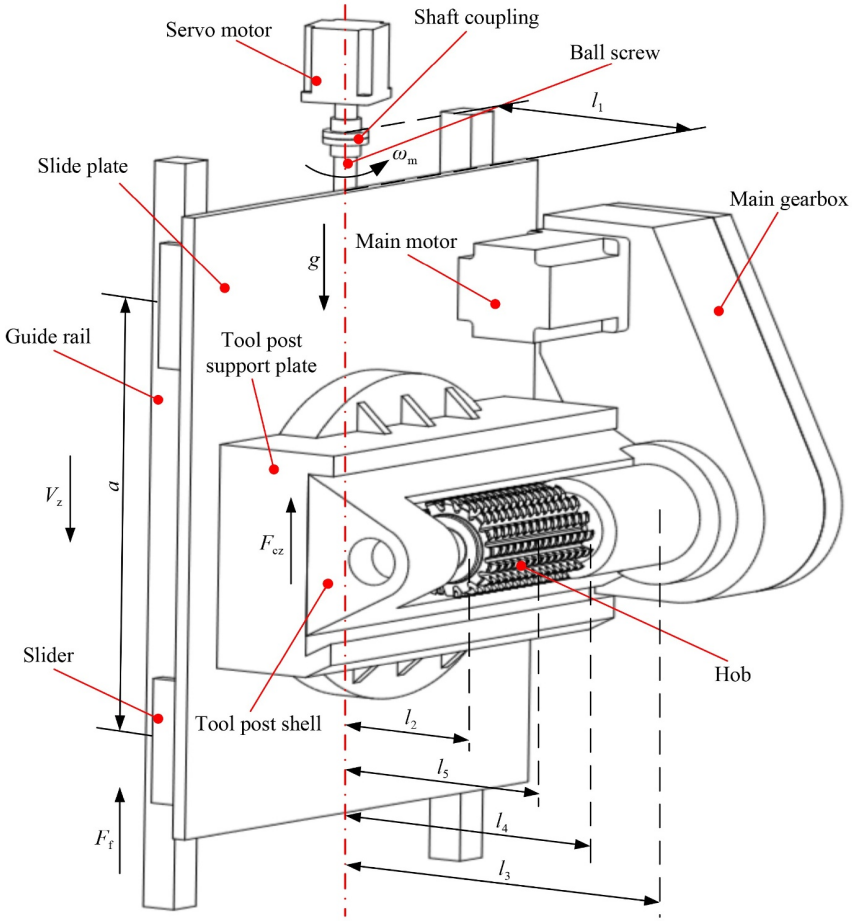

Fig. 2 Structure and force diagram of the machining unit.

drives the rotary motion of the hob spindle through the main transmission box. The output torque of the servo motor is transmitted by the slide plate and drives the tool post, main transmission box, and other additional components to move up and down along the column guide rail.

2.1 Load analysis of the main motor

The power of the machining unit is provided by the main motor and the servo motor. The output power of the main motor includes the output power of the machining unit, the kinetic energy change rate of the mechanical transmission component, and the friction loss of the mechanical transmission, as shown in Eq. (1) [25]:

$$P_{mo} = P_{mec} + \frac{dE_k}{dt} + P_c = M_0\omega_m + B\omega_m^2 + \frac{dE_k}{dt} + \alpha P_c, \quad (1)$$

where P_{mo} is the output power of the main motor, P_{mec} is the mechanical loss power, t is the operation time of the machine tool, dE_k/dt is the rate of change in kinetic energy of mechanical transmission components, P_c is the cutting power, M_0 is the equivalent nonload Coulomb friction moment, B is the equivalent viscous friction damping coefficient, ω_m is the angular velocity of the spindle motor shaft, and α is the load factor of the mechanical transmission system.

When the hobbing machine tool is in a stable state, the kinetic energy E_k change in the mechanical transmission part can be ignored, so the kinetic energy change rate $dE_k/dt = 0$.

The cutting power formula of hobbing is $P_c = F_c \cdot v_c$, and the cutting force F_c is usually calculated by using an empirical formula, which is expressed as Eq. (2) [26]:

$$F_c = 18.2\frac{m^{1.75}Z^{0.27}a_p^{0.81}f_z^{0.65}v_c^{-0.26}K_1K_2K_3}{d_h}, \; v_c = \frac{\pi d_h n_{gm}}{1000}, \quad (2)$$

where Z is the tooth number of the workpiece, f_z is the axial feed of the hob, m is the normal modulus of the hob, a_p is the cut depth, v_c is the cutting speed, n_{gm} is the hob speed, d_h is the hob outer diameter, K_1 is the coefficient associated with materials of the gear, K_2 is the coefficient associated with the hardness of the gear, and K_3 is the coefficient associated with the helical angle of the gear.

2.2 Load analysis of the servo motor

The main gearbox of the machining unit is firmly connected to the tool post. The output torque of the servo

motor drives the tool post, main gearbox, and other additional components along the column to feed up and down along the column through the coupling, ball screw, guide rail, slide block, and skateboard.

The output torque of the motor is mainly used to overcome the friction between the guide rail and the sliding plate, the cutting component force in the feed direction, the gravity and inertial force of the tool post–slide plate module. The force diagram is represented in Fig. 2.

The functional relation between the servo motor output power, output torque, and angular velocity can be expressed as $P_{sm} = T_{sm} \cdot \omega_{sm}$. The power of the transmission system is provided by the servo motor, and the equation is shown in Eq. (3):

$$T_{sm} = J_{sm}\frac{d\omega_{sm}}{dt} + B_{sm}\omega_{sm} + T_l = 2\pi J_{sm}\frac{dn_{sm}}{dt} + 2\pi B_{sm}n_{sm} + T_l, \tag{3}$$

where P_{sm} is the output power of the servo motor, T_{sm} is the output torque of the servo motor, J_{sm} is the moment of inertia of the servo motor, ω_{sm} is the output angular velocity of the servo motor, B_{sm} is the damping coefficient of the servo motor, n_{sm} is the speed of the servo motor, and T_l is the output torque of the coupling.

The servo motor drives the ball screw through the coupling, and the ball screw pair drives the processing unit to move up and down along the column. The dynamic equation of the coupling is expressed as Eq. (4):

$$T_l = J_l\frac{d\omega_{sm}}{dt} + \frac{T_z}{\eta_l} = J_l\frac{d\omega_{sm}}{dt} + \left(J_s\frac{d\omega_{sm}}{dt} + T_b + \frac{T_t}{\eta_b\eta_z}\right)\frac{1}{\eta_l}, \tag{4}$$

where J_l is the moment of inertia of the coupling, J_s is the moment of inertia of the ball screw, T_z is the input torque of the ball screw, T_b is the frictional moment generated by the bearing preload, η_b is the transmission efficiency of the bearing, η_z is the transmission efficiency of the ball screw, and T_t is the output torque of the ball screw.

The output torque of the ball screw can be calculated as Eq. (5):

$$T_t = \frac{L_b \cdot F_t}{2\pi}, \tag{5}$$

where L_b is the lead of the ball screw, and F_t is the load force of the slide plate.

The load force F_t includes the gravity of the sliding plate tool post transmission module, inertial force, friction force of the guide rail, and cutting component force in the feed direction, which can be expressed as

$$\begin{cases} F_t = M\dfrac{dV_z}{dt} + \mathrm{sgn}(V_z)Mg + F_f + F_{cz}, \\ M = M_h + M_t + M_k + M_c + M_a, \end{cases} \tag{6}$$

where M, M_h, M_t, M_k, M_c, and M_a are the masses of the machining unit, slide plate, tool post support plate, tool post shell, main gearbox, and additional components, respectively, F_f is the friction force between the slide plate and the vertical guide rail, F_{cz} is the cutting force on the sliding plate, g is the gravitational acceleration, V_z is the axial feed speed of the moving components along the Z axis, and $V_z = L_b \cdot \omega_{sm}/(2\pi)$.

An integrated model of friction is developed to accurately describe the friction of the sliding plate moving along the Z axis, which can be expressed as

$$F_f = f_v + f_c\mathrm{sgn}(V_z) = \mu_v V_z + \mu_c |F_N| \mathrm{sgn}(V_z), \tag{7}$$

where f_c is the Coulomb friction force, f_v is the viscous friction force, F_N is the normal force on the guide rail, sgn(·) is the symbolic function, μ_c is the Coulomb friction coefficient, and μ_v is the viscous friction coefficient.

The load force on the guide rail is related to many factors, such as the configuration method (horizontal, vertical or oblique), the center of gravity and the force point of the sliding plate, its load-bearing components, and the inertial force at the start and stop. The normal load on the linear motion guide of the system can be expressed as

$$F_N = \frac{1}{2a}\left\{\left(g + \frac{dV_z}{dt}\right)[M_h l_1 + (M_t + M_k) l_2 + M_c l_3 + M_a l_4] + F_{cz} l_5\right\}, \tag{8}$$

where a is the distance between the two sliders, l_1 is the distance between the barycenters of the slide plate and the axis of the ball screw, l_2 is the distance between the barycenters of the tool post and the axis of the ball screw, l_3 is the distance between the barycenters of the main gearbox and the axis of the ball screw, l_4 is the distance between the barycenters of the additional component and the axis of the ball screw, and l_5 is the distance between the barycenters of the hob and the axis of the ball screw.

2.3 Comprehensive energy consumption function

The efficiency of the motor under any working condition is the ratio of output power to input power, which can be expressed as Eq. (9) [23]:

$$\eta(i) = \frac{P_{o\text{-}i}}{P_{n\text{-}i}} = \frac{P_{o\text{-}i}}{P_{o\text{-}i} + P_{loss\text{-}i}},\ P_{o\text{-}i} = \frac{N_i \cdot T_i}{9550}, \tag{9}$$

where $\eta(i)$ is the motor efficiency under working condition i, $P_{o\text{-}i}$ is the motor output power under working condition i, $P_{n\text{-}i}$ is the motor input power under working condition i, N_i is the motor speed under working condition i, T_i is the motor output torque under working condition i, and $P_{loss\text{-}i}$ is the motor loss power under working condition i, which mainly includes copper loss power $P_{Cu\text{-}i}$, eddy current loss power $P_{e\text{-}i}$, hysteresis loss power $P_{h\text{-}i}$, mechanical loss power $P_{m\text{-}i}$, and additional loss power $P_{ad\text{-}i}$.

The peak loss power of the motor and its every part is calculated as Eq. (10) [27]:

$$\begin{cases} P_{\text{loss}} = \dfrac{2}{3} h t_{\text{r}} A, \\ P_{\text{Cu}} = 0.59 P_{\text{loss}}, \\ P_{\text{e}} = P_{\text{h}} = 0.11 P_{\text{loss}}, \end{cases} \tag{10}$$

where P_{loss} is the peak loss power of the motor, P_{Cu} is the peak copper loss power, P_{e} is the peak eddy current loss power, P_{h} is the peak hysteresis loss power, t_{r} is the limit value of temperature rise, A is the surface area of the motor core, and h is the heat dissipation coefficient.

The motor efficiency under working condition i is computed as Eq. (11):

$$\eta(i) = \frac{P_{\text{o-}i}}{P_{\text{o-}i} + P_{\text{Cu-}i} + P_{\text{e-}i} + P_{\text{h-}i} + P_{\text{m-}i} + P_{\text{ad-}i}} = \begin{cases} \dfrac{P_{\text{o-}i}}{P_{\text{o-}i} + 1.064\left[\left(\dfrac{n_{\text{N}} P_{\text{o-}i}}{N_i P_{\max}}\right)^2 P_{\text{Cu}} + \left(\dfrac{N_i}{n_{\text{N}}}\right)^2 P_{\text{e}} + \dfrac{N_i}{n_{\text{N}}} P_{\text{h}} + 1.11 \times 10^{-5} N_i^{0.7} P_{\text{N}}\right]}, & N_i \leqslant n_{\text{N}}, \\ \dfrac{P_{\text{o-}i}}{P_{\text{o-}i} + 1.064\left[\left(\dfrac{P_{\text{o-}i}}{P_{\max}}\right)^2 P_{\text{Cu}} + \left(\dfrac{N_i}{n_{\text{N}}}\right)^{0.6} P_{\text{h}} + P_{\text{e}} + 1.11 \times 10^{-5} N_i^{0.7} P_{\text{N}}\right]}, & N_i > n_{\text{N}}, \end{cases} \tag{11}$$

where n_{N} is the rated speed of the motor, $P_{\max}$ is the peak power, and P_{N} is the rated power.

The comprehensive energy model can be established by analyzing the dynamic equations of the machining unit, as shown in Eq. (12):

$$\begin{aligned} P &= \frac{P_{\text{m}}}{\eta_{\text{m}}} + \frac{P_{\text{sm}}}{\eta_{\text{sm}}} \\ &= \frac{1}{\eta_{\text{m}}}\left(M_0 \omega_{\text{m}} + B\omega_{\text{m}}^2 + 18.2\alpha\pi m^{1.75} Z^{0.27} a_{\text{p}}^{0.81} f_{\text{z}}^{0.65} v_{\text{c}}^{-0.26} K_1 K_2 K_3 n_{\text{gm}}\right) \\ &\quad + \frac{1}{\eta_{\text{sm}}}\left\{2\pi J_{\text{sm}} \frac{\text{d}n_{\text{sm}}}{\text{d}t} + 2\pi B_{\text{sm}} n_{\text{sm}} + J_{\text{l}} \frac{\text{d}\omega_{\text{sm}}}{\text{d}t}\right. \\ &\quad + \frac{1}{\eta_{\text{l}}}\left\{J_{\text{s}} \frac{\text{d}\omega_{\text{sm}}}{\text{d}t} + T_{\text{b}} + \frac{L_{\text{b}}}{2\pi\eta_{\text{b}}\eta_{\text{z}}}\left\{M \frac{L_{\text{b}}}{2\pi} \frac{\text{d}\omega_{\text{sm}}}{\text{d}t} + \text{sgn}(V_z) Mg + F_{\text{cz}} + \mu_{\text{v}} \frac{L_{\text{b}}}{2\pi} \omega_{\text{sm}}\right.\right. \\ &\quad \left.\left.\left. + \frac{\mu_{\text{c}}}{2a}\left\{\left(g + \frac{L_{\text{b}}}{2\pi} \frac{\text{d}\omega_{\text{sm}}}{\text{d}t}\right)\left[M_{\text{h}} l_1 + (M_{\text{t}} + M_{\text{k}}) l_2 + M_{\text{c}} l_3 + M_{\text{a}} l_4\right] + F_{\text{cz}} l_5\right\}\right\}\right\}\right\}, \end{aligned} \tag{12}$$

where η_{m} is the main motor efficiency during operation, η_{sm} is the servo motor efficiency during operation, and P is the power of the machining unit.

The comprehensive energy consumption model can be established through the integration of the power model of the machining unit, which can be expressed as Eq. (13):

$$E = \int_0^t P \text{d}t, \tag{13}$$

where E is the energy consumption of the machining unit.

3 Optimization model of the machining unit

To clearly explain the integrated optimization design method of the machining unit of hobbing machine tool for energy saving, this paper discusses the comprehensive energy consumption modeling and optimization method of the machining unit by taking a YS3118CNC5 hobbing machine tool as an example. The CNC hobbing machine tool and its machining unit are shown in Fig. 3. The main technical data of the machine tool and gear are shown in Table 1. The parameters used for the calculation of the energy consumption in the example are given in Table 2.

The optimization objectives and variables of the machining unit are determined in Section 3.1, followed by the surrogate model for the tool displacement and tool post pallet mass in Section 3.2. The integrated optimization model is built in Section 3.3.

3.1 Determination of the optimization objectives and variables

3.1.1 Optimization objectives

As one of the most important parts of the hobbing machine tool, the machining unit is the main energy-consuming component of the machine tool. The energy consumption of the machining unit, which is expressed in Eq. (13), is determined as one optimization objective.

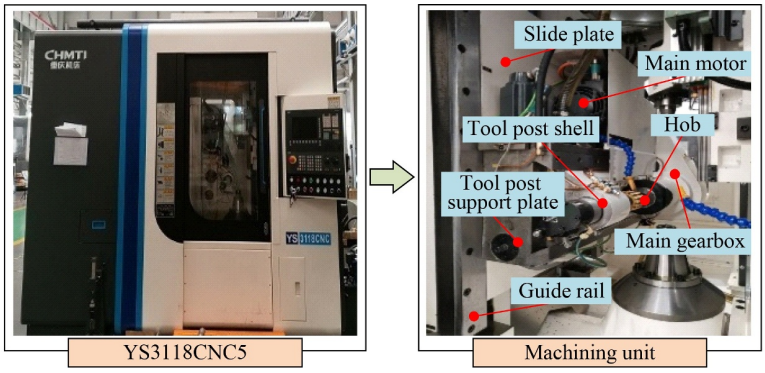

Fig. 3 YS3118CNC5 hobbing machine tool and its machining unit.

Table 1 Main technical parameters of the machine tool and gear

Parameter	Value
Maximum workpiece diameter	180 mm
Maximum processing modulus	4 mm
Maximum axial stroke (Z axis)	285 mm
Diameter of the working table	190 mm
Maximum spindle speed (B axis)	1000 r/min
Total mass of the machine tool	8600 kg
Gear material	AISI 1045 (UNS G10450)
Gear hardness	180 HB
Gear helical angle	20°

The machining unit directly drives the hob to rotate, so the parameters of the machining unit directly affect the maximum offset of the tool during the machining process. In this paper, the maximum offset of the tool is represented by the moving distance of the hob center point, which is called the tool displacement, as shown in Fig. 4. The tool displacement measures the machining accuracy and error of the machining unit, and is determined as another optimization objective.

3.1.2 Optimization variables

In accordance with the analysis in Section 2, the rated power of the main motor (P_{N1}), the peak power of the main motor (P_{max1}), the rated speed of the main motor (n_{N1}), the rated power of the servo motor (P_{N2}), the peak power of the servo motor (P_{max2}), and the rated speed of the servo motor (n_{N2}) are selected as the optimization variables.

Some structures of the tool post support plate are assembled with other components, and the dimensional parameters between them need to be matched with each other, including the diameters of some holes and the overall dimension, so these structure parameters cannot be changed. The parameters of the tool post support plate that can be adjusted, such as x_1, x_2, x_3, x_4, and x_5, are selected as the optimization variables, as shown in Fig. 5.

Table 2 Parameters used for the calculation of energy consumption

Equation	Parameter	Value
Eq. (1)	M_0	198.54 N·m
	B	0.3
	α	0.2
Eq. (2)	m	20 mm
	K_1	1
	K_2	1.05
	K_3	1.11
	d_h	290 mm
Eq. (3)	J_{sm}	4×10^{-4} kg·m^2
	B_{sm}	0.12
Eq. (4)	J_l	3.287×10^{-3} kg·m^2
	T_b	5 N·m
	η_b	0.98
	η_z	0.9
	η_l	0.99
Eq. (5)	L_b	4 mm
Eq. (6)	M_h	100 kg
	M_k	200 kg
	M_c	150 kg
	M_a	50 kg
Eq. (7)	μ_v	0.3
	μ_c	0.3
Eq. (8)	a	0.7 m
	l_1	0.05 m
	l_2	0.2 m
	l_3	0.271 m
	l_4	0.235 m
	l_5	0.221 m
Eq. (10)	h	50
	t_r	40 °C
	A	0.2435 m^2

3.2 Optimization objective function

In this section, the simulation experiment based on Latin hypercube sampling (LHS) is designed, and the surrogate models of the tool post support plate mass (M_t) and tool displacement (δ) are established on the basis of experimental data. The surrogate model of δ is selected as the objective function of the tool displacement. The surrogate model of M_t is used in the comprehensive energy consumption function to calculate the objective of the energy consumption.

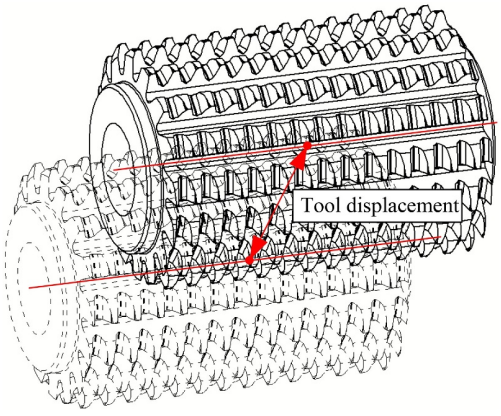

Fig. 4 Schematic of tool displacement of the hobbing machine tool.

3.2.1 Simulation experiment design

LHS method is used to design the simulation experiment for obtaining the sample point data of 60 sets of the structure parameters of the tool post support plate [28]. The distribution of sample point data is shown in Fig. 5. The sample points of the design variables are evenly distributed in the design space and have good characteristics of filling and balance.

On the basis of each group of the design variables of the tool post support plate shown in Fig. 6, the corresponding 3D model of the hobbing machine tool is established on Solidworks software. The 3D model is

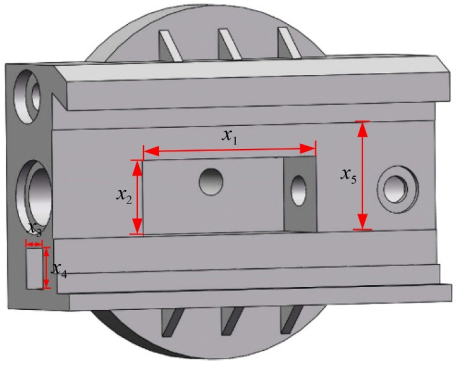

Fig. 5 Tool post support plate of the machining unit.

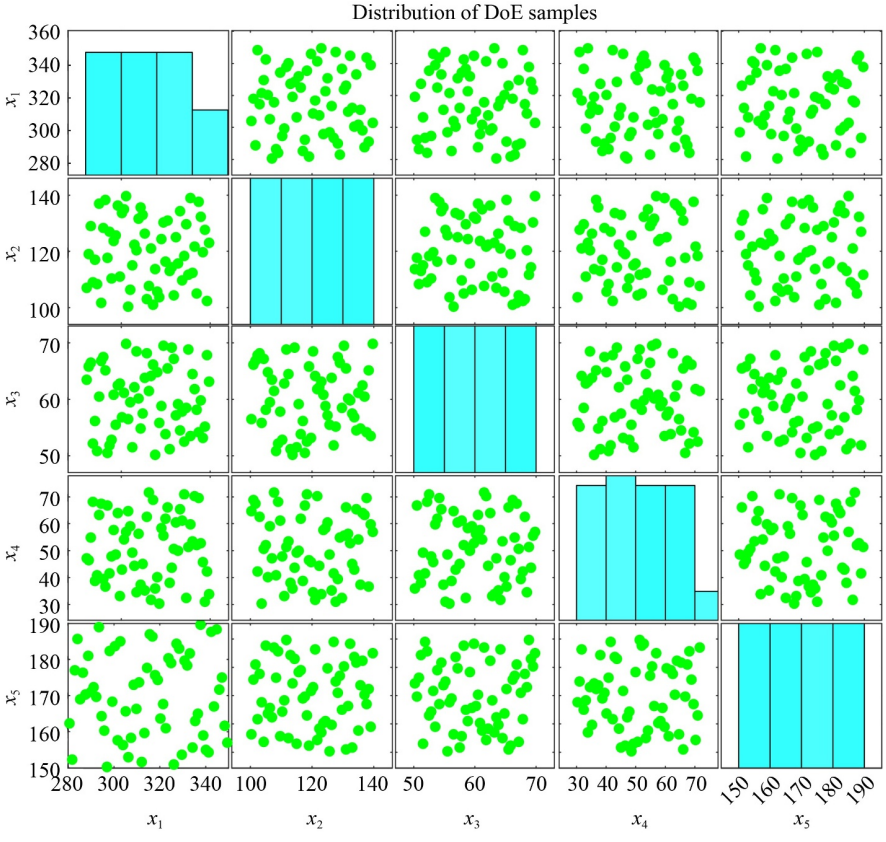

Fig. 6 Distribution of sample points of the design variables in the LHS experiment. DoE: design of experiment.

imported to ANSYS Workbench software to build a finite element model.

The static analysis of the tool post support plate is conducted by using the rigid−flexible coupling method to obtain the tool displacement affected by the deformation of the tool holder pallet. In the simulation analysis, the tool post support plate is treated with flexibility, and the remaining components are treated with rigidity to obtain the finite element model of the hobbing machine tool, as shown in Fig. 7.

The original mass of the hobbing machine tool is 6779.8 kg, the original volume is 9.6854×10^8 mm^3, and the material is structural steel in ANSYS Workbench. The mesh shape of the machining unit is tetrahedron, the mesh size is 30 mm, the number of meshes is 12333, and the number of nodes is 20360. The direction of gravity is the Y positive direction. The value and direction of the load are −2027 N in the X direction, 13990 N in the Y direction, and 3279 N in the Z direction.

The data of the design variables obtained by the LHS experiment and the data of M_t and δ computed by the finite element model are shown in Table 3. The descriptive statistics of the dataset of the LHS experiment are described in Table 4.

3.2.2 Surrogate model establishment

A comparative study of three modeling methods, namely Kriging, RBF, and RSM, is conducted to determine the suitable modeling method for the optimization objectives. The three methods are commonly used to establish surrogate models [29].

RSM is a traditional fitting method to obtain the response value corresponding to the level of each factor by regression fitting and response surface and contour line drawing, and the optimal response values can be predicted. It is suitable for problems with a small amount

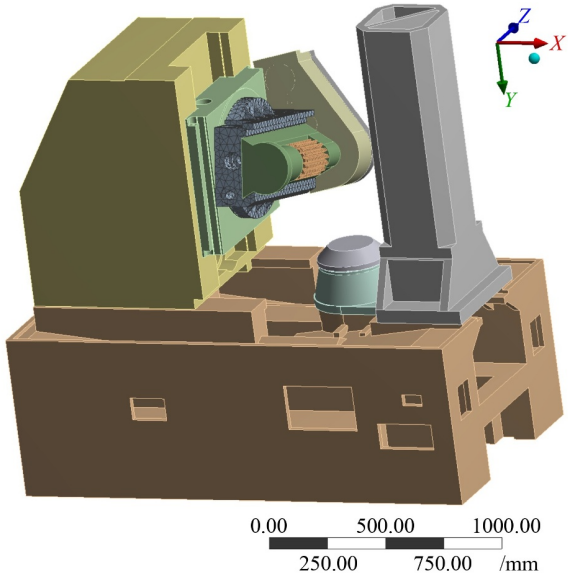

Fig. 7 Finite element model of the hobbing machine tool.

Table 3 Dataset of the LHS experiment

Experiment No.	Design variable					Simulation value	
	x_1/mm	x_2/mm	x_3/mm	x_4/mm	x_5/mm	M_t/kg	δ/(10^{-4} mm)
1	303.91	100.33	56.50	64.65	156.33	216.5745	4.263
2	316.75	121.00	64.17	31.75	186.33	216.4166	3.948
3	281.75	119.00	65.83	46.45	152.33	215.4793	4.167
…	…	…	…	…	…	…	…
58	326.08	131.00	65.50	66.05	151.00	208.8849	4.732
59	308.58	120.33	68.50	34.55	173.00	216.0139	4.041
60	347.08	127.67	55.17	31.05	175.00	214.5871	3.942

Table 4 Descriptive statistics of the dataset of the LHS experiment. The number of samples for each parameter was 60

Value type	Design variable					Simulation value	
	x_1/mm	x_2/mm	x_3/mm	x_4/mm	x_5/mm	M_t/kg	δ/(10^{-4} mm)
Mean	315.00	120.00	60.00	51.00	170.00	213.9898	4.237
Standard deviation	20.20	11.55	5.77	12.12	11.55	3.0322	0.257
Minimum	280.58	100.33	50.17	30.35	150.33	208.6802	3.680
1st quartile	297.79	110.17	55.09	40.68	160.17	211.7175	4.048
Median	315.00	120.00	60.00	51.00	170.00	214.1703	4.235
3rd quartile	332.21	129.84	64.92	61.33	179.84	215.8750	4.443
Maximum	349.42	139.67	69.83	71.65	189.67	221.3104	4.730

of data. The common second-order polynomial of RSM can be expressed as

$$y = \hat{y} = \xi_0 + \sum_{i=1}^{n} \xi_i x_i + \sum_{i=1}^{n} \sum_{j>i}^{n} \xi_{ij} x_i x_j + \sum_{i=1}^{n} \xi_{ii} x_i^2, \tag{14}$$

where $\hat{y}$ is the fitting expression of y, ξ_0, ξ_i, and ξ_{ij} are undetermined coefficients of the RSM model, and x_i and x_j are the sample points.

RBF is a modeling method of surrogate models that combines a series of precise interpolation methods to generate a smooth surface from a large number of data points to predict random processes based on basis functions. It has strong generalization and multidimensional nonlinear mapping ability [30]. The RBF model can be formulated as

$$\begin{cases} y = \hat{y} = \sum_{i=1}^{n} \varpi_i \kappa(\|x_i - \chi\|) + \ell(\boldsymbol{x}), \\ \boldsymbol{x} = (x_1, x_2, ..., x_n), \end{cases} \tag{15}$$

where ϖ_i is the adaptability weight coefficient, $\kappa(\cdot)$ is the RBF, $\|\cdot\|$ is the Euclidean norm, χ is the center of $\kappa(\cdot)$, $\ell(\cdot)$ is the linear polynomial function, and $\boldsymbol{x}$ is the sample data set.

Kriging is suitable for fitting and modeling nonlinear problems [31]. The Kriging model can be denoted as

$$\begin{cases} y = \varsigma(\boldsymbol{x}) + \Theta(\boldsymbol{x}), \\ \operatorname{cov}\left[\Theta\left(\boldsymbol{x}^{(i)}, \boldsymbol{x}^{(j)}\right)\right] = \hbar^2 \Xi\left[\Xi\left(\boldsymbol{x}^{(i)}, \boldsymbol{x}^{(j)}\right)\right], \end{cases} \tag{16}$$

where $\varsigma(\cdot)$ is the global prediction polynomial, $\Theta(\cdot)$ is the random error and its mean is zero, $\hbar^2$ is the variance of $\Theta(\cdot)$, and $\Xi(\cdot)$ is the correlation function. In this work, the Gaussian function is used as the correlation function, as shown in Eq. (17):

$$\Phi\left(\boldsymbol{x}^{(i)}, \boldsymbol{x}^{(j)}\right) = \prod_{k=1}^{m} \exp\left(-\vartheta_k \left\|\boldsymbol{x}_k^{(i)} - \boldsymbol{x}_k^{(j)}\right\|^2\right), \tag{17}$$

where ϑ_k is the related parameter determined by maximum likelihood estimation.

The mean absolute error (MAE), root mean square error (RMSE), and R-square (R^2) are taken to evaluate the accuracy of the surrogate models. The smaller the value of MAE and RMSE, the closer the predicted value to the observed value. The value range of R^2 is between 0 and 1. The closer the value of R^2 is to 1, the higher the prediction accuracy of the model. The expressions of these three indicators are shown as

$$\begin{cases} \mathrm{MAE} = \sum_{i=1}^{N_s} \dfrac{\left|\gamma_i - \gamma_i^*\right|}{N_s}, \\ \mathrm{RMSE} = \sqrt{\sum_{i=1}^{N_s} \dfrac{(\gamma_i - \gamma_i^*)^2}{N_s}}, \\ R^2 = 1 - \dfrac{\sum_{i=1}^{N_s} (\gamma_i - \gamma_i^*)^2}{\sum_{i=1}^{N_s} (\gamma_i - \bar{\gamma}_i)^2}, \end{cases} \tag{18}$$

where N_s is the number of samples, γ_i is the ith observed value, γ_i^* is the ith predicted value, and $\bar{\gamma}_i$ is the mean value of the ith observed value.

In the LHS experiment, 60 sets of data are randomly divided into two groups. The 50 sets of data are defined as the training set, and the remaining 10 sets of data are defined as the test set. Six surrogate models of M_t and δ are established by the RSM, RBF, and kriging methods based on the training set. The accuracy and extensiveness of the six surrogate models are tested.

The test results of the surrogate models are shown in Fig. 8. The results indicate that M_t adopts the RSM method with the highest accuracy, and δ adopts the RBF method with higher accuracy. Therefore, RSM is selected to build the surrogate model of M_t, and the RBF is chosen to build the surrogate model of δ.

The surrogate model of M_t is a multiple quadratic regression equation based on RSM, as shown below:

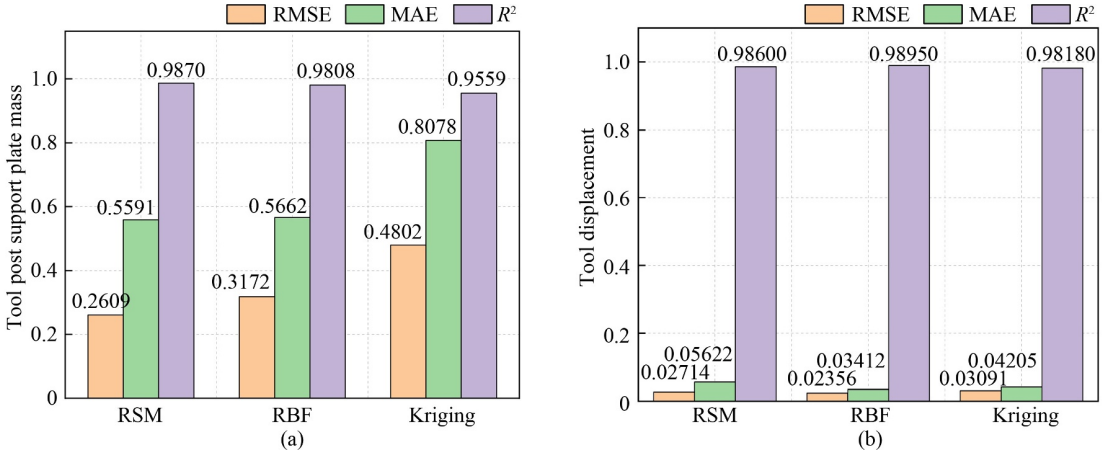

Fig. 8 Test results of the surrogate models of (a) tool post support plate mass and (b) tool displacement.

$$\begin{aligned}\mathrm{RSM}(M_\mathrm{t}) &= \xi_0+\xi_1x_1+\xi_2x_2+\cdots+\xi_{55}x_5^2\\ &= \xi_0+\begin{bmatrix} a_1 & a_2 & a_3 & a_4 & a_5\\ a_{11} & a_{12} & a_{13} & a_{14} & a_{15}\\ 0 & a_{22} & a_{23} & a_{24} & a_{25}\\ 0 & 0 & a_{33} & a_{34} & a_{35}\\ 0 & 0 & 0 & a_{44} & a_{45}\\ 0 & 0 & 0 & 0 & a_{55}\end{bmatrix}\begin{bmatrix} x_1 & x_1^2 & 0 & 0 & 0 & 0\\ x_2 & x_1x_2 & x_2^2 & 0 & 0 & 0\\ x_3 & x_1x_3 & x_2x_3 & x_3^2 & 0 & 0\\ x_4 & x_1x_4 & x_2x_4 & x_3x_4 & x_4^2 & 0\\ x_5 & x_1x_5 & x_2x_5 & x_3x_5 & x_4x_5 & x_5^2\end{bmatrix} = \xi_0+\boldsymbol{\xi}_{6\times5}\boldsymbol{X}_{5\times6},\end{aligned} \tag{19}$$

where $\xi_0 = 286.243$, $\boldsymbol{\xi}_{6\times5} =$

$$\begin{bmatrix} -0.026 & -0.469 & 0.099 & -0.395 & -0.061\\ 2.3\times10^{3} & 1.1\times10^{-4} & 1.6\times10^{-3} & 5.5\times10^{-4} & 1.2\times10^{-3}\\ 0 & -7.1\times10^{-5} & 2.5\times10^{-4} & -5.4\times10^{-4} & -2.6\times10^{-4}\\ 0 & 0 & -3.0\times10^{-3} & 8.7\times10^{-5} & -5.1\times10^{-5}\\ 0 & 0 & 0 & -1.9\times10^{-5} & -7.4\times10^{-5}\\ 0 & 0 & 0 & 0 & -1.4\times10^{-4}\end{bmatrix}.$$

The surrogate model of δ is an RBF neural network, which is a three-layer neural network, including an input layer, a hidden layer, and an output layer. The key parameters of the RBF neural network are the synaptic weight matrix $\boldsymbol{\varpi}_{50\times1}$ and the output threshold vector $\boldsymbol{T}$, as shown in

$$\begin{cases}\boldsymbol{\varpi}_{50\times1} = \begin{bmatrix}-1.36\times10^{-8} & 2.63\times10^{-7} & 1.11\times10^{-8} & \cdots & 1.74\times10^{-6} & 3.52\times10^{-8} & 6.61\times10^{-5}\end{bmatrix}^\mathrm{T},\\ \boldsymbol{T} = \left(2.07\times10^{-7},\ 6.98\times10^{-7},\ 1.83\times10^{-6},\ 1.74\times10^{-6},\ 3.52\times10^{-8},\ 6.61\times10^{-5}\right)^\mathrm{T}.\end{cases} \tag{20}$$

3.3 Integrated optimization model

The constraints of the processing are analyzed, and the integrated optimization model of the machining unit is established to ensure that the hobbing machine tool can still meet the processing requirements after optimization.

The processing parameters of gear hobbing directly affect the machining capacity and efficiency [32]. The processing parameters corresponding to the optimized motor parameters, including the axial feed of hob, the hob speed, and the depth of cut, should be within the reasonable range allowed by normal machining to ensure the machining capacity and efficiency of gear hobbing, as shown in

$$\begin{cases} f_{z\min} \leqslant f_z \leqslant f_{z\max},\\ n_{gm\min} \leqslant n_{gm} \leqslant n_{gm\max},\\ a_{p\min} \leqslant a_p \leqslant a_{p\max}.\end{cases} \tag{21}$$

The total power consumed by the machine tool cutting must be within the range that the motor can provide, that is, the cutting power must be less than the maximum power of the motor, as shown in

$$\frac{18.2}{\eta_\mathrm{m}}m^{1.75}Z^{0.27}a_\mathrm{p}^{0.81}f_\mathrm{z}^{0.65}v_\mathrm{c}^{0.76}\frac{K_1K_2K_3}{d_\mathrm{h}} \leqslant P_{\max1}. \tag{22}$$

During the acceleration period of the main motor and servo motor of the gear hobbing machine tool, the maximum rotational power should not exceed the rated power of the motor, as shown in

$$\begin{cases} P_\mathrm{SA} = P_\mathrm{SR} + J_\mathrm{s}^*\alpha^*\omega^* \leqslant P_\mathrm{N},\\ \alpha^* = \dfrac{2\pi f_\mathrm{BA}}{pt_\mathrm{A}},\\ \omega^* = \dfrac{2\pi n^*}{60} + \dfrac{2\pi f_\mathrm{BA}t^*}{pt_\mathrm{A}},\end{cases} \tag{23}$$

where P_SA is the motor acceleration power, P_SR is the motor shaft rotation power, J_s^* is the moment of inertia equivalent to the motor shaft of the transmission system, p is the number of pole pairs of the motor, α^* is the motor angular acceleration, ω^* is the angular velocity of the motor, n^* is the initial speed before the motor is accelerated, f_BA is the basic frequency of the inverter, t_A is the acceleration time of the inverter, and t^* is the duration of the rotation acceleration.

The natural frequency can well represent the dynamic characteristics of the machine tool, so the optimized frequency of the machine tool needs to meet the constraint shown in

$$f_i \geqslant [f_i], \tag{24}$$

where f_i is the ith order natural frequency of the machine tool after optimization, $[f_i]$ is the ith order natural frequency before optimization, and $i = 1,2,...,6$.

On the basis of the comprehensive energy consumption function and the surrogate model establishment, the optimization objective of the energy consumption E is obtained by inputting the surrogate model of M_t into the energy consumption function, and the optimization objective of the tool displacement δ is obtained by the surrogate model of δ. The optimization variables are the 11 parameters of the structure and the motors.

An integrated optimization model is established, as shown in

$$\begin{aligned}&\min F(\boldsymbol{\Lambda}_1,\boldsymbol{\Lambda}_2) = (\min E(\boldsymbol{\Lambda}_1,\boldsymbol{\Lambda}_2), \min \delta(\boldsymbol{\Lambda}_2)),\\ &\boldsymbol{\Lambda}_1 = (P_{N1}, P_{\max1}, n_{N1}, P_{N2}, P_{\max2}, n_{N2}),\\ &\boldsymbol{\Lambda}_2 = (x_1, x_2, x_3, x_4, x_5),\end{aligned}$$

$$\text{s.t.:}\begin{cases} f_{z\min} \leqslant f_z \leqslant f_{z\max}, \\ n_{gm\min} \leqslant n_{gm} \leqslant n_{gm\max}, \\ a_{p\min} \leqslant a_p \leqslant a_{p\max}, \\ \dfrac{18.2m^{1.75}Z^{0.27}a_p^{0.81}f_z^{0.65}v_c^{0.76}K_1K_2K_3}{d_h\eta_m} \leqslant P_{\max 1}, \\ P_{SA} = P_{SR} + J_s^*\alpha^*\omega^* \leqslant P, \\ f_i \geqslant [f_i]. \end{cases} \tag{25}$$

4 Optimization algorithm and result analysis

The multiobjective particle swarm optimization (MOPSO) algorithm is used to optimize the integrated optimization model of the machining unit of the hobbing machine tool. The optimization results are analyzed and discussed.

4.1 Optimization algorithm

The MOPSO algorithm has the advantages of fast convergence speed, good convergence effect, and easy realization [33], which is suitable to address the multiobjective optimization problem in this paper. The parameters of the MOPSO algorithm are shown in Table 5. The main program of the algorithm is provided as follows.

Procedure: the MOPSO algorithm

1. **For** each particle *i*
2. Initialize *Dim*-dimensional velocity *Vi* and position *Xi* for particle *i* under the constraint
3. Calculate the fitness values *E*, *δ* for particle *i* and set *pBesti* = *Xi*
4. Initial screening noninferior solutions to archive
5. **End for**
6. **For** *j* = 1 to *Mit* do
7. **For** *i* = 1 to *Nip* do
8. Update velocity *Vi* and position *Xi* for particle *i*
9. Calculate the fitness values *E* and *δ* for particle *i*
10. **If** *E*(*Xi*) < *E*(*pBesti*) and *δ*(*Xi*) < *δ*(*pBesti*)
11. *pBesti* = *Xi*
12. **End if**
13. **End for**
14. Update noninferior solutions to archive
15. **End for**
16. Output noninferior solution set archive

End

4.2 Optimization result and discussion

4.2.1 Optimization result

The simulation and computation are implemented on a computer workstation with Intel Core i9-10900K CPU at 3.70 GHz and 64 GB RAM. Three Pareto solutions are selected from the two ends and the middle of the Pareto frontier, as shown in Fig. 9. The details of these solution sets are shown in Table 6.

The results show that the energy consumption of the first solution is the smallest, and the tool displacement meets the constraint. For practical machining, the machining accuracy needs to symbolize the process requirements, and higher accuracy does indicate better results. Under the condition of meeting the machining accuracy, the smaller the energy consumption, the better. Hence the first solution is selected as the final optimal solution.

4.2.2 Discussion of the result

The energy consumption and tool displacement are optimized as the single objective to discuss the optimization effect of the machining unit. The simulation analysis results are illustrated in Fig. 10, and the comparison of the results is shown in Table 7.

The optimization results indicate that when the energy consumption is taken as the single objective, the energy consumption decreases from 3.122×10^9 to 1.661×10^9 J, which is a 46.8% reduction, but the tool displacement is larger than before. When the tool displacement is taken as the single objective, the tool displacement is reduced from 0.00039290 to 0.00034553 mm, which is a 12.1% reduction, but the energy consumption is larger than before. When taking the energy consumption and tool displacement as optimization objectives, the energy

Table 5 Relevant parameters of the MOPSO

Algorithm setting	Symbol	Value
Particle dimension	*Dim*	11
Initial population number	*Nip*	100
Maximum iteration number	*Mit*	300
Learning factor	c_1	2
	c_2	2
Inertia weight	ω_{ini}	0.9
	ω_{end}	0.4

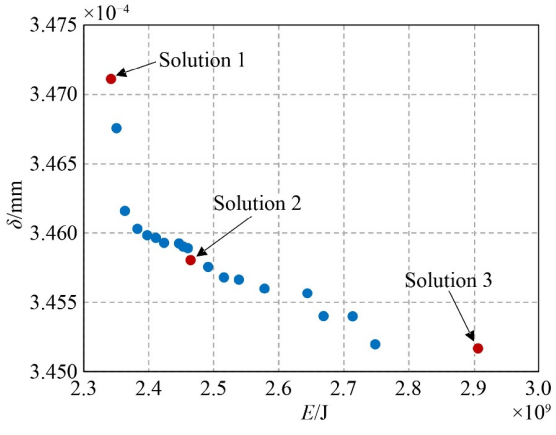

Fig. 9 Pareto frontier of the optimization results of the MOPSO algorithm.

Table 6 Solutions selected from the Pareto frontier. They have the same parameters, i.e., P_{N1} = 3000 W, n_{N1} = 800 r/min, P_{N2} = 1500 W, x_2 = 100 mm, x_3 = 50 mm, and x_4 = 30 mm

Pareto solution	Optimization variable					Optimization objective	
	Main motor parameter	Servo motor parameter		Structure parameter			
	P_{max1}/W	P_{max2}/W	n_{N2}/(r·min^{-1})	x_1/mm	x_5/mm	E/(10^9 J)	δ/(10^{-4} mm)
1	6552	9321	540	288	171	2.342	3.4711
2	6052	11892	500	280	165	2.465	3.4582
3	4930	11855	500	280	152	2.907	3.4518

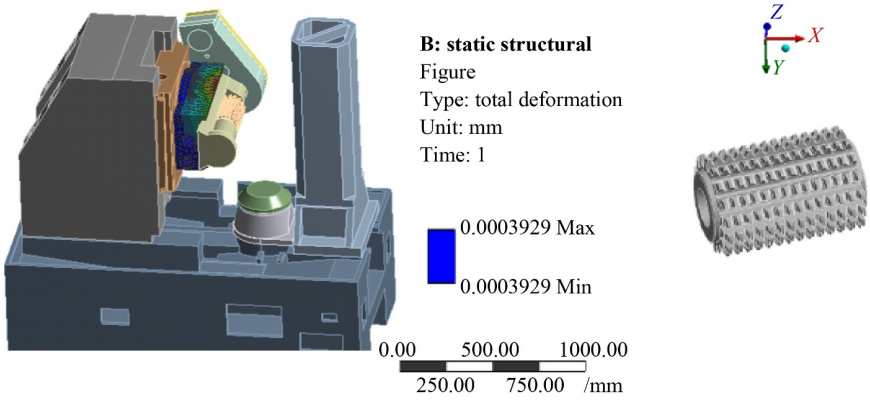

Fig. 10 Tool displacement simulation result of the original value.

Table 7 Comparison of variables and objectives before and after the optimization

Optimization type	Optimization variable											Optimization objective	
	Main motor parameter			Servo motor parameter			Structure parameter						
	P_{N1}/W	P_{max1}/W	n_{N1}/(r·min^{-1})	P_{N2}/W	P_{max2}/W	n_{N2}/(r·min^{-1})	x_1/mm	x_2/mm	x_3/mm	x_4/mm	x_5/mm	E/(10^9 J)	δ/(10^{-4} mm)
Original value	5000	8000	1000	1800	6000	700	293	112	50	60	160	3.122	3.9290
min(E, δ)	3000	6552	800	1500	9321	540	288	100	50	30	171	2.342	3.4711
min(δ)	5000	8000	1000	1800	6000	700	280	100	50	30	150	3.123	3.4553
min(E)	3000	11000	800	1500	10,000	500	350	140	70	72	190	1.661	4.3719

consumption decreases from 3.122×10^9 to 2.342×10^9 J (i.e., 25.0% reduction), and the tool displacement is reduced from 0.00039290 to 0.00034711 mm (i.e., 11.7% reduction).

In summary, the proposed integrated optimization method can achieve energy saving while optimizing tool displacement. The feasibility of the integrated optimization method is verified.

Sensitivity analysis is a type of analysis that is intended to describe the relative sensitivity of a model's outputs to each of its input variables/parameters [34]. It can rank the importance of input factors at all levels [35]. A sensitivity analysis is conducted to analyze the degree of influence of different optimization variables on energy consumption and displacement. The results of the sensitivity of each variable are shown in Fig. 11.

As shown in Fig. 11(a), the sensitivity of P_{N1}, P_{N2}, n_{N1}, and n_{N2} to energy consumption is greater than 0, which indicates that the energy consumption is positively correlated with the four variables. When the motor is working normally, its power is the rated power. The higher the rated power of the motor (P_{N1} and P_{N2}), the higher the power and energy consumption of the motor in normal operation, so the higher the energy consumption of the machining unit. P_{N1} has a greater influence on energy consumption than P_{N2} because the rated power of the main motor is higher than that of the servo motor. The higher the rated speed of the motor (n_{N1} and n_{N2}), the higher its rated power, so the higher the energy consumption. The influence of n_{N1} and n_{N2} on energy consumption is similar because the speed of the main motor is close to that of the servo motor.

The sensitivity of P_{max1}, P_{max2}, x_1, x_2, x_3, x_4, and x_5 to energy consumption is smaller than 0, which indicates that the energy consumption is negatively correlated with the seven variables. When the machining unit starts, the corresponding motor will run at the peak power (P_{max1}, P_{max2}). When the running speed is reached, the motor will

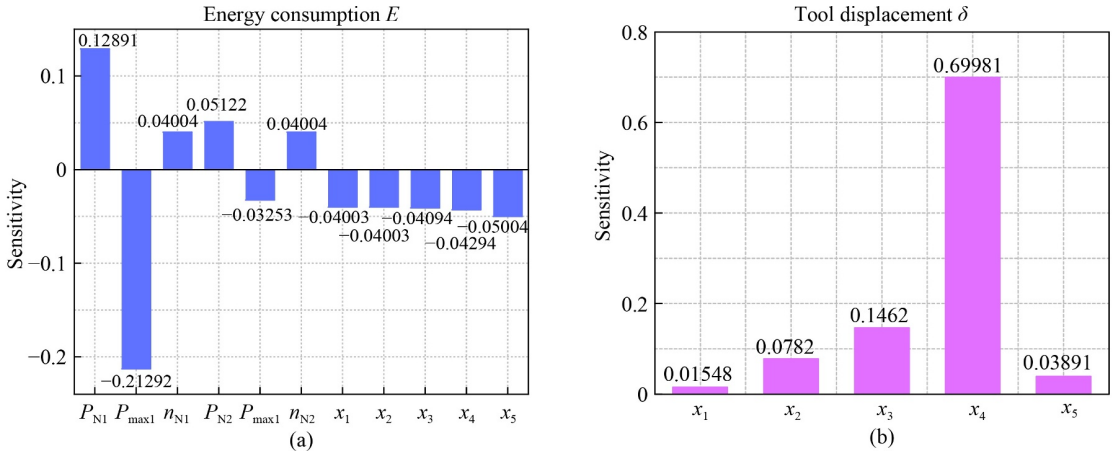

Fig. 11 Sensitivity analysis of (a) energy consumption and (b) tool displacement.

return to the rated power. When the peak power of the motor is higher, the starting time of the machining unit will be shorter, the energy consumption in the starting phase will be smaller, and the total energy consumption will be smaller. As shown in Fig. 5, the larger the structure parameters (x_1, x_2, x_3, x_4, x_5) of the tool post support plate, the larger the hollowed volume and the smaller the actual volume, that is, the smaller the mass of the tool post support plate. Thus, energy consumption decreases.

The motor parameters barely affect the tool displacement, so the sensitivity of x_1, x_2, x_3, x_4, and x_5 is analyzed in Fig. 11(b). The sensitivity is greater than 0, which indicates that the tool displacement is positively correlated with the five variables. In accordance with the previous analysis, the increase in the structure parameters of the tool post support plate increases the hollowed volume and decreases the mass, which can reduce the stiffness and stability of the tool post support plate, so the tool displacement increases.

The 3D surface plots of each group of the variables are drawn to analyze the influence trend of the optimization variables on the optimization objectives, as shown in Figs. 12 and 13, and each group contains two variables.

As shown in Figs. 12(a) and 12(b), the energy consumption increases with the increase in P_{N1}, whereas the energy consumption decreases with the increase in P_{max1} and P_{max2}. In accordance with the shape of the surface, P_{max1} has more influence on energy consumption than P_{N1} and P_{max2}. Figure 12(c) shows that the increase in n_{N1} and n_{N2} causes the increase in energy consumption, and the flat surface indicates that they have a close degree of influence on energy consumption. Figures 12(d)–12(f) show that the energy consumption decreases with the increase in x_1, x_2, x_3, x_4, and x_5. The graph in the figure is approximated as a plane, which indicates that the influence of the five structure parameters on the energy consumption is close.

As shown in Fig. 13, the tool displacement increases with the increase in x_1, x_2, x_3, x_4, and x_5, which is in accordance with the results of the sensitivity analysis. x_2 has a more remarkable effect on the tool displacement than x_5 by comparing Figs. 13(a) and 13(b). Figure 13(c) illustrates that the influence of x_2 on the tool displacement is greater than that of x_5. Similarly, Fig. 13(d) shows that the influence of x_4 on the tool displacement is greater than that of x_3.

In accordance with the above analysis, the patterns of influence of the optimization variables on the objectives are consistent with the conclusions obtained from the sensitivity analysis. The optimization of the motor parameters has great importance on the energy saving of the machining unit.

Although the influence of the single structure parameters on the tool displacement is positive, an appropriate combination of the structure parameters can reduce the tool displacement while reducing energy consumption. In the optimization design of the machining unit, the influence of variables on objectives is intercoupling, so selecting the optimal combination of variables based on design requirements is critical. The machine tool can be as energy efficient as possible while ensuring machining accuracy by reasonably selecting the combination of parameters.

5 Conclusions

An integrated optimization method of the machining unit of the hobbing machine tool is proposed in this paper to achieve the energy saving design while maintaining machining accuracy. The energy consumption function of the machining unit of a hobbing machine tool is established, the energy consumption and tool displacement are taken as the optimization objectives, and the appropriate methods are chosen to build the surrogate models. An energy saving design method for the machining unit that comprehensively considers the energy consumption and

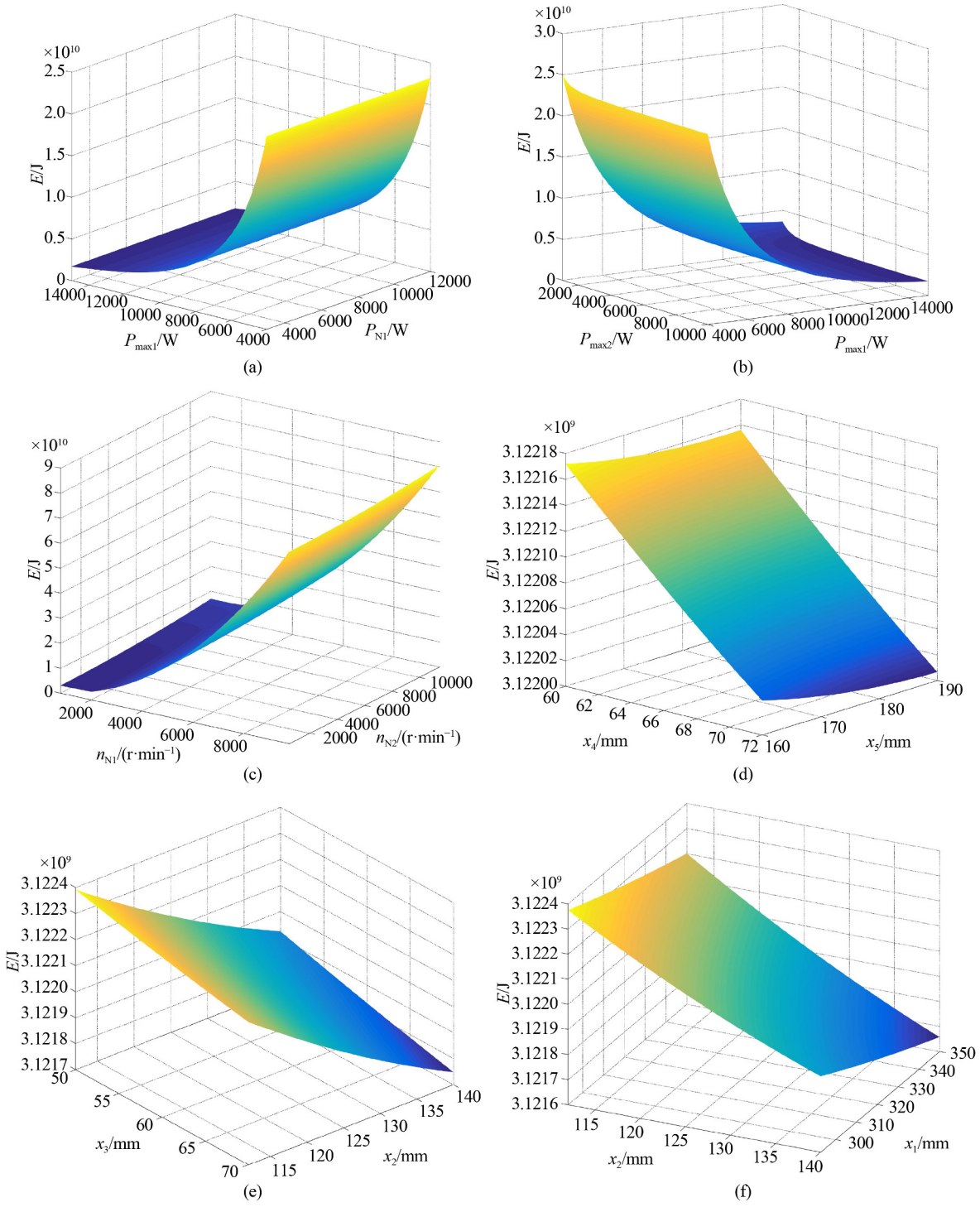

Fig. 12 Influence trend of the variables on the energy consumption: (a) P_{max1} and P_{N1}, (b) P_{max1} and P_{max2} ,(c) n_{N1} and n_{N2}, (d) x_4 and x_5, (e) x_3 and x_2, and (f) x_2 and x_1.

tool displacement is proposed.

The results show that the integrated optimization design method of the machining unit achieves energy saving and reduces the tool displacement. The energy consumption is reduced by 7.80×10^8 J, and the tool displacement is reduced by 4.579×10^{-5} mm through the multiobjective optimization. The energy consumption and tool displacement of the optimized machining unit decrease by 25.0% and 11.7% from the original values, respectively. The sensitivity of the optimization variables on the objectives is analyzed. The values of sensitivity indicate that P_{N1} and P_{max1} have the greatest influence on the energy consumption, and x_4 has the greatest influence on tool displacement. The influence trend of the optimization

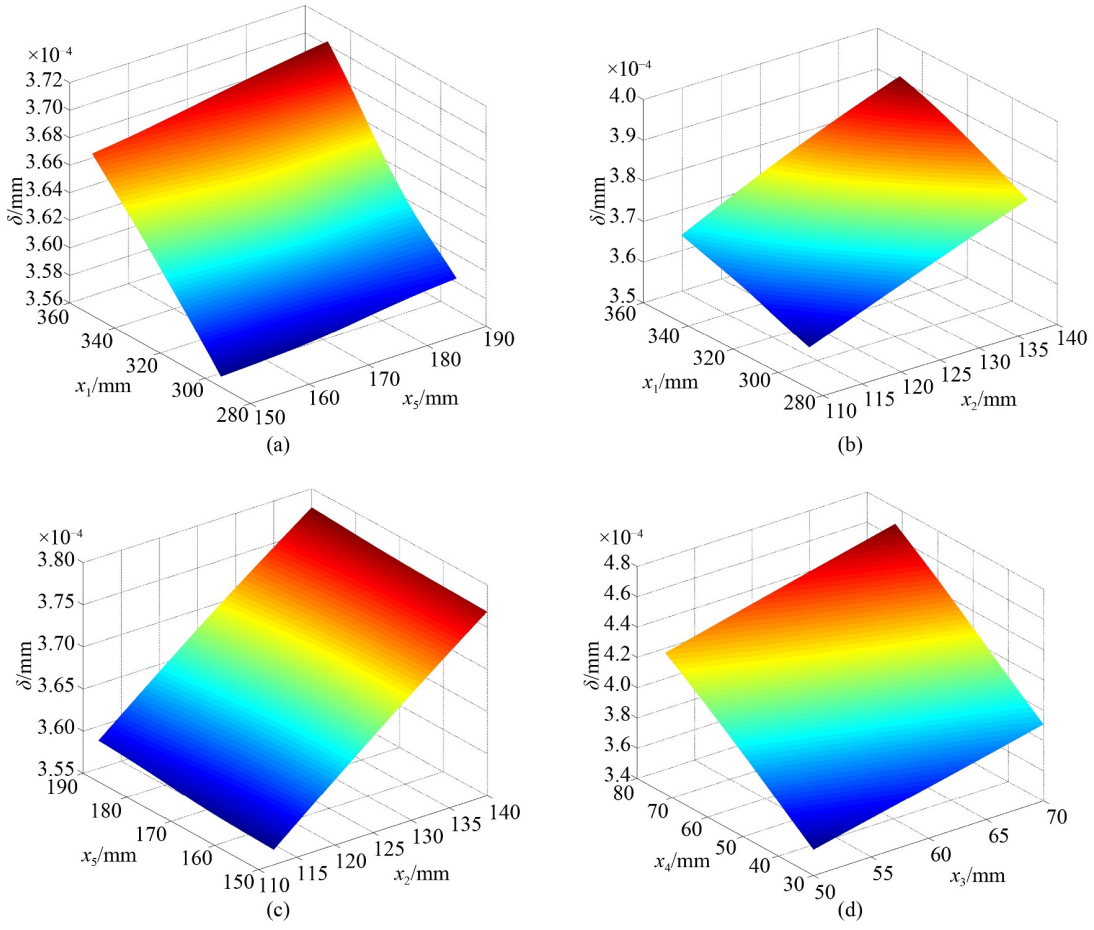

Fig. 13 Influence trend of the variables on the tool displacement. (a) x_1 and x_5, (b) x_1 and x_2, (c) x_5 and x_2, and (d) x_4 and x_3.

variables on the objectives is discussed.

Adaptive sequential sampling will be used to improve the accuracy of surrogate models in future research. The energy consumption function for the whole machine tool will be established.

Nomenclature

a	Distance between the two sliders
a_p	Cut depth
A	Surface area of the motor core
B	Equivalent viscous friction damping coefficient
B_{sm}	Servo motor damping coefficient
c_1, c_2	Learning factors
d_h	Hob outer diameter
Dim	Particle dimension
E	Energy consumption of the machining unit
E_k	Kinetic energy of mechanical transmission components
f_{BA}	Basic frequency of the inverter
f_c	Coulomb friction force
f_i	ith order natural frequency of the machine tool after optimization
$[f_i]$	ith order natural frequency before optimization
f_v	Viscous friction force
f_z	Axial feed of the hob
F_c	Cutting force
F_{cz}	Cutting force on the slide plate
F_f	Friction force between the sliding plate and the vertical guide rail
F_N	Normal force on the guide rail
F_t	Slide plate load force
g	Gravitational acceleration
h	Heat dissipation coefficient
J_l, J_s, J_{sm}	Moments of inertia of the coupling, ball screw, and servo motor, respectively
J_s^*	Moment of inertia equivalent to the motor shaft of the transmission system
K_1, K_2, K_3	Coefficients associated with the materials, hardness, and helical angle of the gear, respectively
l_1	Distance between the barycenters of the slide plate and the axis of the ball screw

l_2	Distance between the barycenters of the tool post and the axis of the ball screw
l_3	Distance between the barycenters of the main gearbox and the axis of the ball screw
l_4	Distance between the barycenters of the additional component and the axis of the ball screw
l_5	Distance between the barycenters of the hob and the axis of the ball screw
L_b	Ball screw lead
m	Normal modulus of the hob
M, M_a, M_c, M_h, M_k, M_t	Masses of the machining unit, additional components, main gearbox, slide plate, tool post shell, and tool post support plate, respectively
M_0	Equivalent nonload Coulomb friction moment
Mit	Maximum iteration number
n^*	Initial speed before the motor is accelerated
n_{gm}	Hob speed
n_N	Rated speed of the motor
n_{N1}, n_{N2}	Rated speeds of the main and servo motors, respectively
n_{sm}	Servo motor speed
N_i	Motor speed under working condition i
Nip	Initial population number
N_s	Number of samples
p	Number of pole pairs of the motor
P	Power of the machining unit
$P_{ad\text{-}i}$	Additional loss power under working condition i
P_c	Cutting power
P_{Cu}	Peak copper loss power
$P_{Cu\text{-}i}$	Copper loss power under working condition i
P_e	Peak eddy current loss power
$P_{e\text{-}i}$	Eddy current loss power under working condition i
P_h	Peak hysteresis loss power
$P_{h\text{-}i}$	Hysteresis loss power under working condition i
P_{loss}	Peak loss power of the motor
$P_{loss\text{-}i}$	Motor loss power under working condition i
$P_{m\text{-}i}$	Mechanical loss power under working condition i
P_{max}	Peak power of the motor
P_{max1}, P_{max2}	Peak powers of the main and servo motors, respectively
P_{mec}	Mechanical loss power
P_{mo}	Main motor output power
$P_{n\text{-}i}$	Motor input power under working condition i
P_N	Rated power
P_{N1}	Rated power of the main motor
P_{N2}	Rated power of the servo motor
P_{sm}	Servo motor output power
$P_{o\text{-}i}$	Motor output power under working condition i.
P_{SA}	Motor acceleration power
P_{SR}	Motor shaft rotation power
sgn(·)	Symbolic function
t	Operation time of the machine tool.
t^*	Duration of the rotation acceleration
t_A	Acceleration time of the inverter
t_r	Limit value of temperature rise
T_b	Frictional moment generated by the bearing preload
T_i	Motor output torque under working condition i
T_l	Coupling output torque
T_{sm}	Servo motor output torque
T_t	Output torque of the ball screw
T_z	Input torque of the ball screw
$\boldsymbol{T}$	Output threshold vector
v_c	Cutting speed
V_z	Axial feed speed of the moving components along the Z axis
$\boldsymbol{x}$	Sample data set
x_i, x_j	Sample points
x_1, x_2, x_3, x_4, x_5	Structure parameters of the tool post support plate
$\hat{y}$	Fitting expression of y
Z	Tooth number of the workpiece
α	Load factor of the mechanical transmission system
α^*	Motor angular acceleration
γ_i	ith observed value
γ_i^*	ith predicted value
$\bar{\gamma}_i$	Mean value of the ith observed value
δ	Tool displacement
$\varsigma(\cdot)$	Global prediction polynomial
$\Theta(\cdot)$	Random error
$\kappa(\cdot)$	Radial basis function
η_b	Bearing transmission efficiency
η_m, η_{sm}	Motor efficiencies of the main and servo motors, respectively
η_z	Ball screw transmission efficiency
$\eta(i)$	Motor efficiency under working condition i
μ_c	Coulomb friction coefficient
μ_v	Viscous friction coefficient
χ	Center of $\kappa(\cdot)$
ω^*	Angular velocity of the motor
ω_{end}, ω_{ini}	Final and initial values of the inertia weight, respectively
ω_m	Angular velocity of the spindle motor shaft
ω_{sm}	Servo motor output angular velocity
ξ_0, ξ_i, ξ_{ij}	Undetermined coefficients of the RSM model
$\ell(\cdot)$	Linear polynomial function
$\hbar^2$	Variance of $\Theta(\cdot)$
$\Xi(\cdot)$	Correlation function
ϑ_k	Related parameter determined by the maximum likelihood estimation
ϖ_i	Adaptability weight coefficient

$\boldsymbol{\varpi}_{50\times1}$	Synaptic weight matrix
$\|\cdot\|$	Euclidean norm

Acknowledgements This work was supported in part by the National Natural Science Foundation of China (Grant Nos. 51975075 and 52105506) and the Chongqing Technology Innovation and Application Program, China (Grant No. cstc2020jscx-msxmX0221).

References

1. Triebe M J, Zhao F, Sutherland J W. Genetic optimization for the design of a machine tool slide table for reduced energy consumption. Journal of Manufacturing Science and Engineering, 2021, 143(10): 101003
2. Zhong Q Q, Tang R Z, Peng T. Decision rules for energy consumption minimization during material removal process in turning. Journal of Cleaner Production, 2017, 140(3): 1819–1827
3. Papetti A, Menghi R, Di Domizio G, Germani M, Marconi M. Resources value mapping: a method to assess the resource efficiency of manufacturing systems. Applied Energy, 2019, 249: 326–342
4. Zhao J H, Li L, Wang Y, Sutherland J W. Impact of surface machining complexity on energy consumption and efficiency in CNC milling. The International Journal of Advanced Manufacturing Technology, 2019, 102(9): 2891–2905
5. Apostolos F, Alexios P, Georgios P, Panagiotis S, George C. Energy efficiency of manufacturing processes: a critical review. Procedia CIRP, 2013, 628–633
6. Kara S, Li W. Unit process energy consumption models for material removal processes. CIRP Annals, 2011, 60(1): 37–40
7. Xiao Y M, Jiang Z G, Gu Q, Yan W, Wang R P. A novel approach to CNC machining center processing parameters optimization considering energy-saving and low-cost. Journal of Manufacturing Systems, 2021, 59: 535–548
8. Zhang T, Liu Z Q, Shi Z Y, Xu C H. Investigation on size effect of specific cutting energy in mechanical micro-cutting. The International Journal of Advanced Manufacturing Technology, 2017, 91(5): 2621–2633
9. Xiao Q G, Li C B, Tang Y, Pan J, Yu J, Chen X Z. Multi-component energy modeling and optimization for sustainable dry gear hobbing. Energy, 2019, 187: 115911
10. Li C B, Xiao Q G, Tang Y, Li L. A method integrating Taguchi, RSM and MOPSO to CNC machining parameters optimization for energy saving. Journal of Cleaner Production, 2016, 135: 263–275
11. Vu N C, Dang X P, Huang S C. Multi-objective optimization of hard milling process of AISI H13 in terms of productivity, quality, and cutting energy under nanofluid minimum quantity lubrication condition. Measurement and Control, 2021, 54(5–6): 820–834
12. Nguyen T T, Nguyen T A, Trinh Q H. Optimization of milling parameters for energy savings and surface quality. Arabian Journal for Science and Engineering, 2020, 45(11): 9111–9125
13. Arriaza O V, Kim D W, Lee D Y, Suhaimi M A. Trade-off analysis between machining time and energy consumption in impeller NC machining. Robotics and Computer-Integrated Manufacturing, 2017, 43: 164–170
14. Sihag N, Sangwan K S. A systematic literature review on machine tool energy consumption. Journal of Cleaner Production, 2020, 275: 123125
15. Li B, Tian X T, Zhang M. Modeling and multi-objective optimization method of machine tool energy consumption considering tool wear. International Journal of Precision Engineering and Manufacturing-Green Technology, 2022, 9(1): 127–141
16. Zhang X W, Yu T B, Dai Y X, Qu S, Zhao J. Energy consumption considering tool wear and optimization of cutting parameters in micro milling process. International Journal of Mechanical Sciences, 2020, 178: 105628
17. He K Y, Tang R Z, Jin M Z. Pareto fronts of machining parameters for trade-off among energy consumption, cutting force and processing time. International Journal of Production Economics, 2017, 185: 113–127
18. Kumar R, Bilga P S, Singh S. Multi objective optimization using different methods of assigning weights to energy consumption responses, surface roughness and material removal rate during rough turning operation. Journal of Cleaner Production, 2017, 164: 45–57
19. Yoon H S, Kim E S, Kim M S, Lee J Y, Lee G B, Ahn S H. Towards greener machine tools—a review on energy saving strategies and technologies. Renewable and Sustainable Energy Reviews, 2015, 48: 870–891
20. Triebe M J, Zhao F, Sutherland J W. Achieving energy efficient machine tools by mass reduction through multi-objective optimization. Procedia CIRP, 2019, 80: 73–78
21. Ji Q Q, Li C B, Zhu D G, Jin Y, Lv Y, He J X. Structural design optimization of moving component in CNC machine tool for energy saving. Journal of Cleaner Production, 2020, 246: 118976
22. Lv J X, Tang R Z, Tang W C J, Liu Y, Zhang Y F, Jia S. An investigation into reducing the spindle acceleration energy consumption of machine tools. Journal of Cleaner Production, 2017, 143: 794–803
23. Wójcicki J, Bianchi G. Electric load management in spindle run-up and run-down for multi-spindle machine tools via optimal power-torque trajectories and peak load synchronization. The International Journal of Advanced Manufacturing Technology, 2018, 95(5): 1819–1835
24. Denkena B, Abele E, Brecher C, Dittrich M A, Kara S, Mori M. Energy efficient machine tools. CIRP Annals, 2020, 69(2): 646–667
25. Liu S, Liu F, Hu S H, Yin Z B. Energy survey of machine tools: separating power information of the main transmission system during machining process. Journal of Advanced Mechanical Design, Systems, and Manufacturing, 2012, 6(4): 445–455
26. Liu X, Zhao F, Mei X S. A fuzzy adaptive controller for constant cutting torque in high-performance gear hobbing process. In: Proceedings of 2017 IEEE International Conference on Advanced Intelligent Mechatronics (AIM). Munich: IEEE, 2017, 1725–1730
27. Hall E, Ramamurthy S S, Balda J C. Optimum speed ratio of induction motor drives for electrical vehicle propulsion. In: Proceedings of APEC 2001 the 16th Annual IEEE Applied Power Electronics Conference and Exposition (Cat. NO.01CH37181).

Anaheim: IEEE, 2001, 371–377

28. Afzal A, Kim K Y, Seo J W. Effects of Latin hypercube sampling on surrogate modeling and optimization. International Journal of Fluid Machinery and Systems, 2017, 10(3): 240–253
29. Li C B, Li Y S, Gao L, Garg A, Li W. Surrogate model-based heat dissipation optimization of air-cooling battery packs involving herringbone fins. International Journal of Energy Research, 2021, 45(6): 8508–8523
30. Amouzgar K, Strömberg N. Radial basis functions as surrogate models with a priori bias in comparison with a posteriori bias. Structural and Multidisciplinary Optimization, 2017, 55(4): 1453–1469
31. Kleijnen J P C. Regression and Kriging metamodels with their experimental designs in simulation: a review. European Journal of Operational Research, 2017, 256(1): 1–16
32. Ni H X, Yan C P, Ni S F, Shu H, Zhang Y. Multi-verse optimizer based parameters decision with considering tool life in dry hobbing process. Advances in Manufacturing, 2021, 9(2): 216–234
33. Paul D, Jain A, Saha S, Mathew J. Multi-objective PSO based online feature selection for multi-label classification. Knowledge-Based Systems, 2021, 222: 106966
34. Oliveira B, Ballio F, Maia R. Numerical modelling-based sensitivity analysis of fluvial morphodynamics. Environmental Modelling & Software, 2021, 135: 104903
35. Xu C, Zhu P, Liu Z, Tao W. Mapping-based hierarchical sensitivity analysis for multilevel systems with multidimensional correlations. Journal of Mechanical Design, 2021, 143(1): 011707